UDK 691.73:54.057:669.333.2
Original scientific article/Izvirni znanstveni članek

ISSN 1580-2949
MTAEC9, 57(4)359(2023)

TWO-STEP SYNTHESIS AND FORMATION MECHANISM FOR LACUOS NANO-SIZED AGGLOMERATES

DVOSTOPENJSKA SINTEZA IN MEHANIZEM TVORBE LACUOS NANOAGLOMERATOV

Xing Li*, Qiang Li, Zhenning Ma, Yan Sun

Shenyang Jianzhu University, Department of Science, Shenyang, 110168, P.R. China

Prejem rokopisa – received: 2023-05-14; sprejem za objavo – accepted for publication: 2023-06-21

doi:10.17222/mit.2023.879

We have developed a two-step synthesis method to obtain pure LaCuOS nano-sized agglomerates using $La(NO_3)_3{\cdot}6H_2O$, $CuSO_4{\cdot}5H_2O$ and $NH_3{\cdot}H_2O$ as the starting materials. The result shows that the precursor can be converted into $La_2O_2SO_4$, $La_2(SO_4)_3$ and CuO phases at 800 °C for 2 h in air, which was then converted into a pure LaCuOS phase by a reduction at 800 °C for 5 h in a flowing argon and hydrogen atmosphere. The as prepared LaCuOS nano-aggregates have poor dispersion and a wide size distribution range (50–100 nm).

Keywords: lanthanide copper oxychalcogenide, two-step synthesis, co-precipitation, reduction

Avtorji opisujejo razvoj metode dvostopenjske sinteze za izdelavo čistega LaCuOSv obliki nanoaglomeratov. Kot izhodiščne materiale so uporabili $La(NO_3)_3{\cdot}6H_2O$, $CuSO_4{\cdot}5H_2O$ in $NH_3{\cdot}H_2O$. Rezultati analiz so pokazali, da se ta prekurzor oziroma izhodiščne materiale lahko pretvori v fazo $La_2O_2SO_4$, $La_2(SO_4)_3$ in CuO pri 800 °C po 2 urah segrevanja na zraku. Pretvorbo v čisto LaCuOS fazo pa so potem izvedli z redukcijo pri 800 °C po 5 urah segrevanja v reduktivni mešanici argona in vodika. Izdelani nanoagregati LaCuOS so imeli dokaj obsežno porazdelitev velikosti delcev med 50 nm in 100 nm.

Ključne besede:bakrov oksihalogenidni lantanid, dvostopenjska sinteza, koprecipitacija, redukcija

1 INTRODUCTION

Quaternary-layered oxychalcogenides with the general formula LnCuOQ (Ln=lanthanides and Q=S, Se), recently termed the "1 1 1 1" structure, are known to exhibit interesting structures and exciting physical properties, such as ionic conductivity, transparency, coupled with semiconductivity, and medium-temperature superconductivity.[1,2] In particular, it is a crucial and well-known challenge to develop a wide-gap p-type semiconductor, which was already applied to ultraviolet-green light-emitting diodes (LEDs) utilizing pn junctions, full-color LEDs or white LEDs.[3,4] Interest in rare-earth Cu-based oxychalcogenides, typical layered oxysulfide LaCuOS with a band gap of 3.1 eV, is known to be one of the few transparent, p-type semiconductors and exhibits efficient blue photoluminescence and large third-order optical nonlinearity due to exciton at room temperature.[5] LaCuOS is a mixed-anion material composed of divalent oxygen and sulfur anions. The important feature of its crystal structure is that LaCuOS crystallizes in a layered structure, and Cu^+ ions are coordinated by sulfur anions exclusively. LaCuOS is a tetragonal system (space group: P4/nmm), and its crystal structure is composed of a $(La_2O_2)^{2+}$ oxide layer and $(Cu_2S_2)^{2-}$ sulfide layer stacked alternately along the c-axis. The ionic LaO layers confine the Cu–S bonds in the two-dimensional CuS layers and preserve the transparent quality of LaCuOS.[6–8] This naturally layered crystal structure brings interesting electrical and optical properties to these materials. These features suggest that LaCuOS is a promising material and has received considerable attention, owing to the potential optoelectronic application as the active or contact layers of light-emitting devices in ultraviolet and/or blue region, an efficient transparent anode for OLEDs and other photocathode, as well as for use as transparent p-type electrodes.[9–16]

Several different routes have been proposed to prepare different forms of lanthanide copper oxychalcogenide compounds, including oxidization,[16] vacuum solid-state reaction (VSSR),[17] sulfurization,[18] flux,[19–20] heteroepitaxial growth,[21–23] sputtering,[24] and so on. For example, Palazzi prepared the layered oxysulfide LaCuOS by the oxidization of $LaCuS_2$ for the first time in 1981. Yosuke Goto also prepared the LaCuOS by VSSR with La, Cu, S and La_2O_3 as the starting materials. Thus, it is difficult to obtain the product with nano size and good morphology, and at the same time, it raise costs and high-risk safe concerns during the synthesis process.[17] Moreover, VSSR is a complicated preparation process, which needs high temperatures and a long reaction time, and is very energy-intensive. In 2017, with the use of Cu_2O, La_2O_3 and S starting materials, high-quality LaCuOS was synthesized by a solid state-reaction followed by sulfurization.[18] Although Lian et al. briefly reported about the synthesis of LaCuOS nanopowder by a precipitation combined with reduction route,[25] its formation mechanism has not yet been examined in detail.

*Corresponding author's e-mail:
syjz_lixing1979@163.com

Based on these facts, it is necessary to systematically explore the synthesis and formation mechanism of LaCuOS. In this study we have developed a two-step synthesis for preparing pure LaCuOS nano-sized agglomerates and this method has the characteristics of safe, simple, efficient, economical, ease of mass production and is environment friendly. Moreover, we also reported the results of Fourier transform infrared spectra, X-ray diffraction, thermogravimetric analysis, morphologies and energy-dispersive spectroscopy.

2 EXPERIMENTAL PROCEDURES

2.1 Materials and synthesis

$La(NO_3)_3{\cdot}6H_2O$ (AR), $CuSO_4{\cdot}5H_2O$ (AR) and $NH_3{\cdot}H_2O$ (AR) reagents were purchased from Sinopharm Chemical Reagent Co. Ltd., China and used as the starting materials without further purification. Firstly, 0.1-M $La(NO_3)_3$ and $CuSO_4$ solutions were obtained by dissolving a stoichiometric amount of $La(NO_3)_3{\cdot}6H_2O$ and $CuSO_4{\cdot}5H_2O$ in deionized water, respectively. The mother liquor was obtained by mixing the above $La(NO_3)_3$ and $CuSO_4$ solutions according to a molar ratio of 1:1:1 for La^{3+}:Cu^{2+}:SO_4^{2-}. The 3-M $NH_3{\cdot}H_2O$ solution was prepared by dissolving stronger ammonia water into deionized water and used as the precipitant. Secondly, the precursor was prepared by dropping the precipitant solution at a rate of 2 mL·min^{-1} into the mother liquor under vigorous stirring at room temperature. During the co-precipitation process, the pH value of the reaction system was continuously monitored with the ZDJ-4B automatic potentiometric titrator. After dropping, the resulting light-blue precipitate was aged for 2 h, and then separated and washed repeatedly with deionized water to obtain the precursor. The precursor was then dried at 80 °C for 12 h and calcined at different temperatures for 2 h in air. Thirdly, the calcined powder was pressed into 16-mm-diameter disks by bidirectional uniaxial compaction under 100 MPa. Finally, the powder compact was placed in a tubular furnace and reduced at specific temperatures (450 °C and 800 °C) for 5 h in the hybrid atmosphere of flowing hydrogen and argon (90 % Ar + 10 % H_2), followed by furnace cooling to room temperature.

2.2 Characterization

The titration curve was recorded with a Shanghai ZDJ-4B automatic potentiometric titrator. Fourier-transform infrared spectra (FTIR) were obtained in the region 4000–400 cm^{-1} using an Agilent Cary 660 FTIR spectrophotometer and the KBr method. The phase structures were identified by X-ray diffractometer (XRD, D8 Advance) operating at 40 kV and 30 mA with Cu-K_α (0.15406 nm) radiation. Thermogravimetry (TG), derivative thermogravimetry (DTG) and differential thermal analysis (DTA) were performed using simultaneous differential thermal analysis and thermo-gravimetry (SDT 2960). The particle morphologies and energy-dispersive spectroscopy (EDS) pattern were obtained on a JEOL-2010 TEM at an acceleration of 200 kV.

3 RESULTS AND DISCUSSION

3.1 Selection of pH value in co precipitation process

To determine the appropriate ammonia volume and completely precipitate all the La^{3+} and Cu^{2+} ions, the effect of titrated ammonia volume on the pH value in the $La(NO_3)_3$-$NH_3{\cdot}H_2O$, $CuSO_4$-$NH_3{\cdot}H_2O$ and $La(NO_3)_3$-$CuSO_4$-$NH_3{\cdot}H_2O$ systems were investigated, respectively, as shown in **Figure 1**. From **Figure 1a**, with the increase of ammonia to ≈0.08 mL, pH value of $La(NO_3)_3$ solution increases dramatically from an initial 6.15 to 8.27, and at the same time the white precipitate was formed. When the titration amount of ammonia water continues to increase, the pH value of $La(NO_3)_3$-$NH_3{\cdot}H_2O$ system increases slowly and shows an approximate plateau around 8.30–9.00, which is attributed to La^{3+} ions reacting with OH^- groups completely. The increase of the concentration of OH^- generated by ammonia hydrolysis leads to an increase in pH value with further increasing the volume amount of ammonia water. From **Figure 1b**, the pH value increases from an initial value of 5.13 in the $CuSO_4$-$NH_3{\cdot}H_2O$ system and the blue precipitate was observed in this clear blue solution, corresponding to the following chemical reaction:

$$2CuSO_4 + 2NH_3{\cdot}H_2O = Cu_2(OH)_2SO_4\downarrow + (NH_4)_2SO_4 \quad (1)$$

A titration jump occurred when the volume of ammonia reached ≈2.72 mL with a pH value of 6.00, indicating that the titration endpoint (2.72, 6.00) had been reached. To continue to increase the amount of ammonia water is unfavorable to the precipitate and excessive ammonia water will react with the precipitate, which causes the precipitation to become a dark-blue solution. The corresponding complex reaction can be expressed as follows:

$$CuSO_4 + 4NH_3{\cdot}H_2O = [Cu(NH_3)_4]SO_4 + 4H_2O \quad (2)$$

As can be seen from **Figure 1c**, when the $NH_3{\cdot}H_2O$ volume reaches ≈0.38 mL, the pH value increases from an initial value of 4.58 to 5.22 in the $La(NO_3)_3$-$CuSO_4$-$NH_3{\cdot}H_2O$ system. Then pH value increases slowly from 5.22 to 5.91 when the $NH_3{\cdot}H_2O$ volume reaches ≈2.95 mL, which is the Cu^{2+} ion precipitation interval according to the result of **Figure 1b**, corresponding to equation (1). With continuously increasing $NH_3{\cdot}H_2O$ dosage to ≈5.33 mL, pH amounts to 8.33 at the same time, La^{3+} ion precipitation occurs, javascript:; which is attributed to La^{3+} ions reacting with the OH^- and SO_4^{2-} groups. The reaction concerning the La^{3+} ion precipitation can be expressed as follows:

$$2La^{3+} + SO_4^{2-} + 4OH^- + xH_2O = La_2(OH)_4SO_4{\cdot}xH_2O \quad (3)$$

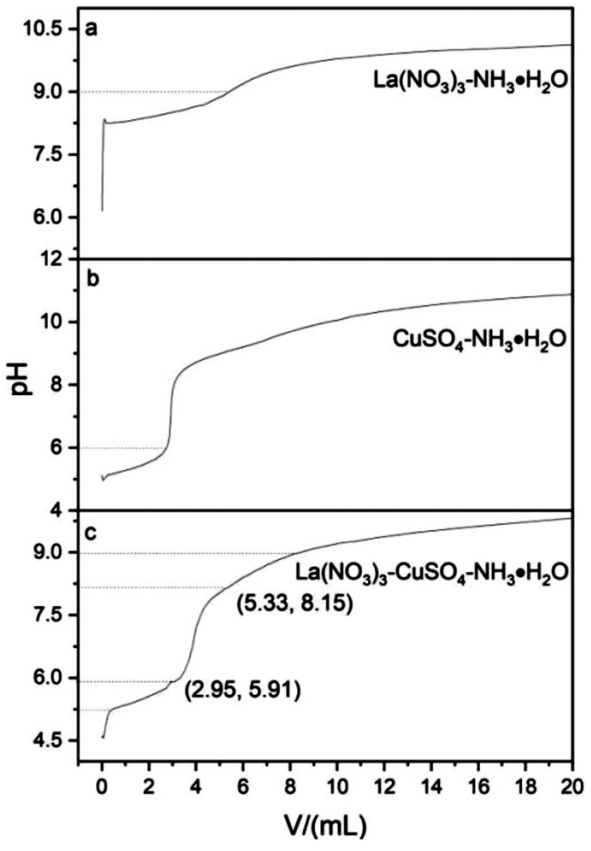

Figure 1: Titration curves for : a) $La(NO_3)_3$-$NH_3{\cdot}H_2O$, b) $CuSO_4$-$NH_3{\cdot}H_2O$, c) $La(NO_3)_3$-$CuSO_4$-$NH_3{\cdot}H_2O$ systems

In the chemical formula (3), the SO_4^{2-} and the OH^- groups derive from the hydrolysis of $CuSO_4$ and $NH_3{\cdot}H_2O$, respectively. Here, the SO_4^{2-}, the OH^- groups are hard bases and the La^{3+} ion is a hard acid, thus the SO_4^{2-} and OH^- groups prefer to coordinate with La^{3+} ions more easily to form $La_2(OH)_4SO_4$ according to the HSAB (hard-soft acid-base) principle.[26] Moreover, the yield of blue precipitation shows the increment tendency with increasing pH value. However, a minor pH value change can be observed on the pH value curve when the $NH_3{\cdot}H_2O$ volume is greater than 8.87 mL. In this work, 8.87 mL of $NH_3{\cdot}H_2O$ is considered the best ammonia volume and the appropriate pH value is 9.00 in $La(NO_3)_3$-$CuSO_4$-$NH_3{\cdot}H_2O$ co-precipitation system.

3.2 FTIR analyses of three precursors

To qualitatively determine the functional group composition of three precursors synthesized by three different systems, i.e., $La(NO_3)_3$-$NH_3{\cdot}H_2O$, $CuSO_4$-$NH_3{\cdot}H_2O$ and $La(NO_3)_3$-$CuSO_4$-$NH_3{\cdot}H_2O$, FTIR analyses were carried out, as displayed in **Figure 2**. The FTIR spectroscopy confirms the presence of the OH^- and NO_3^- groups in the synthesized precursor based on $La(NO_3)_3$-$NH_3{\cdot}H_2O$ system (**Figure 2a**). The vibration peaks at 3520 cm^{-1} and 1640 cm^{-1} are originated from the O–H stretching vibration and the H–O–H bending vibration of hydroxy and adsorbed water molecule in the precursor, respectively. The sharp peak located at 1380 cm^{-1} is assigned to the antisymmetric stretching vibration mode of the nitrate group (NO_3^-). Moreover, the weak peak around 540 cm^{-1} can be attributed to the La-O bond absorption. In the $CuSO_4$-$NH_3{\cdot}H_2O$ system, evidence of the presence of sulfate (SO_4^{2-}) and hydroxyl (OH^-) groups in the precursor can be obtained from **Figure 2b**. The observed fundamental vibrations of the sulfate groups (SO_4^{2-}) are located at 1125 (ν_3) and 600 cm^{-1} (ν_4), respectively. Besides the O-H stretching vibration peaks at 3570 cm^{-1} and 3390 cm^{-1} they are also observed in **Figure 2b**. The peak at 875 cm^{-1} is attributed to multiple frequency absorption of the OH^- groups. The above-mentioned results indicate that the precursor is composed of basic copper sulfate. The FTIR spectrum of the synthesized precursor based on the $La(NO_3)_3$-$CuSO_4$-$NH_3{\cdot}H_2O$ system is labeled in **Figure 2c**. The broad absorption band centered at 3455 cm^{-1} and the weak peak centered at 1640 cm^{-1} are attributed to the stretching and bending vibration peaks of the OH^- groups, respectively. Moreover, the peak around 980 cm^{-1} could be assigned to the strong H-bonding in Cu-O-H.[27] The peaks at 1125 cm^{-1} (ν_3) and 600 cm^{-1} (ν_4) are regarded as the stretching modes of the SO_4^{2-} groups. The result is consistent with that of Lian et al. In addition, two weak absorption peaks centered at ≈1500 cm^{-1}

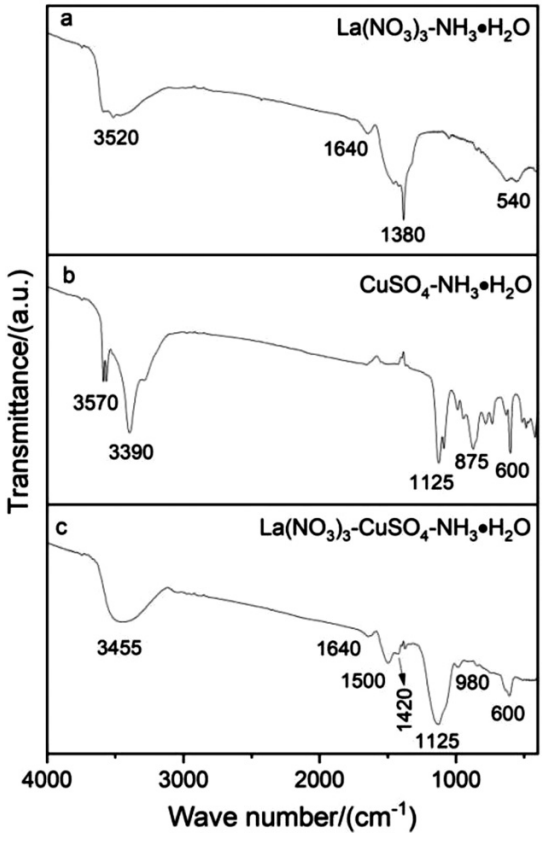

Figure 2: FTIR spectra of three precursors: a) $La(NO_3)_3$-$NH_3{\cdot}H_2O$, b) $CuSO_4$-$NH_3{\cdot}H_2O$, c) $La(NO_3)_3$-$CuSO_4$-$NH_3{\cdot}H_2O$

and 1420 cm^{-1} were unexpectedly observed in the precursor, which can be assigned to the characteristic asymmetrical split stretching of the CO_3^{2-} groups. The trace amount of CO_3^{2-} on the surface of the precursor may be caused by the adsorbed water and carbon dioxide from the ambient atmosphere.

3.3 Thermal analyses of three precursors

To understand the decomposition behavior and determine the optimal calcination temperature for the three precursors, DTA-TG-DTG curves of these precursors were conducted from room temperature to 1000 °C, and these results are shown in **Figure 3**. **Figure 3a** depicts DTA-TG-DTG curve for the synthesized precursor based on the $La(NO_3)_3$-$NH_3{\cdot}H_2O$ system. The TG curve contains three main weight loss steps, and the total weight loss of the precursor is 35.62 *w*/%. The first temperature range of the weight loss is from room temperature to ≈300 °C and a weak endothermic peak centered at ≈50 °C appears on the DTA curve, which is caused by the removal of the crystal water in the precursor. The second weight loss, accompanied by a sharp peak at 343 °C and a weak peak at 522 °C on the DTG curve, is mainly related to the gradual dehydroxylation between ≈300 and ≈600 °C. Besides, a sharp peak at 349 °C and a weak peak at 527 °C appear on the DTA curve, respectively, which indicate that the dehydroxylation process is an endothermic reaction and is carried out step by step.

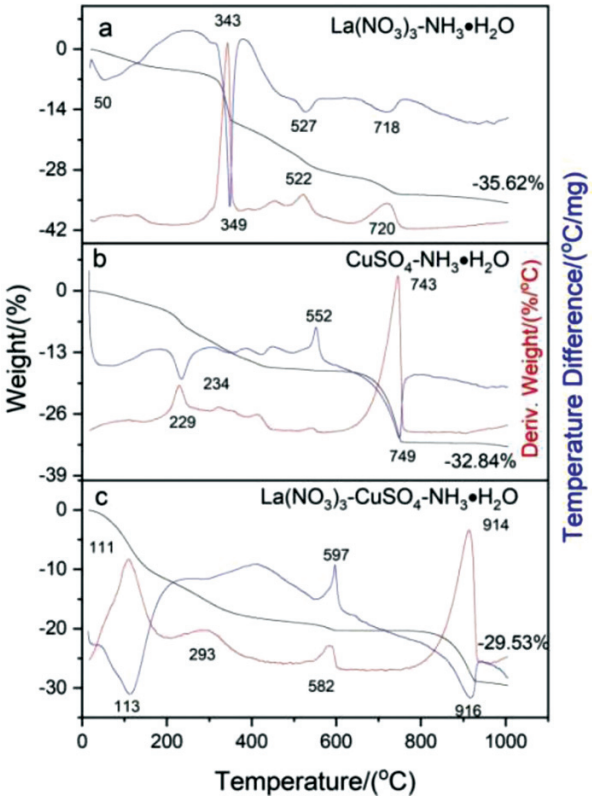

Figure 3: DTA-TG-DTG curves of three precursors: a) $La(NO_3)_3$-$NH_3{\cdot}H_2O$, b) $CuSO_4$-$NH_3{\cdot}H_2O$, c) $La(NO_3)_3$-$CuSO_4$-$NH_3{\cdot}H_2O$

The third weight loss starting at ≈600 °C is caused by the removal of the nitrate group in the precursor with an endothermic peak at 718 °C and DTG maximum value at around 720 °C. Moreover, as shown in **Figure 3a**, little weight changes can be observed at temperatures greater than 800 °C on the TG curve, which indicates that at higher than 800 °C the thermal decomposition is basically finished. The DTA-TG-DTG curve of the synthesized precursor based on $CuSO_4$-$NH_3{\cdot}H_2O$ system is also shown in **Figure 3b**. The TG curve shows a continuous weight loss between room temperature and 1000 °C with an overall weight loss of approximately 32.84 *w*/%. The total weight loss mainly consists of the two following steps in the whole temperature range, as seen from the DTG curve. The first weight loss in the temperature range from room temperature to ≈450 °C is about 16.20 *w*/%, which seems to be related mostly to the removal of adsorbed and hydroxy water from the precursor. This weight loss corresponds to a weak endothermic peak at around 234 °C in the DTA curve, and DTG maxima at about 229 °C in the DTG curve. Moreover, the TG curve shows an approximate plateau between ≈450 and ≈650 °C, accompanied by a upward peak at 552 °C on the DTA curve, suggesting that the crystallization process of $Cu_2(OH)_2SO_4$ phase is an exothermic reaction. The second weight loss starting at ≈600 °C is caused by the complete desulfurization reaction of the $Cu_2(OH)_2SO_4$ phase with an obvious endothermic peak at 749 °C and DTG maximum value at around 743 °C, which corresponds to the following chemical equation (4).

$$CuSO_4{\cdot}CuO = 2CuO + 2SO_2\uparrow + O_2\uparrow \quad (4)$$

Based on the above **Figure 3a** and **3b**, we continued to analyze the thermal decomposition process of the synthesized precursor based on the $La(NO_3)_3$-$CuSO_4$-$NH_3{\cdot}H_2O$ system. As shown in **Figure 3c**, the TG curve shows a continuous weight loss between room temperature and 1000 °C with an overall weight loss of approximately 29.53 *w*/%. According to the DTG curve, the weight loss can be divided into four stages. The first two processes before ≈400 °C are about 18.70 *w*/%, which corresponds to the removal of physically adsorbed and crystal water from the precursor. This weight loss corresponds to an endothermic peak at around 113 °C in the DTA curve, accompanied by a broad peak at 111 °C and a shoulder weak peak at 293 °C on the DTG curve. The third weight loss between 400 °C and 600 °C is about 10.20 *w*/%, which is attributed to the complete dehydroxylation of the precursor. A weak peak appears at 582 °C in DTG curve. At the same time, an obvious exothermic peak around 597 °C in the DTA curve, which may be due to the fact that the exothermic heat of crystallization is greater than the endothermic in dehydroxylation process. The fourth weight loss is at temperatures greater than 800 °C, with an obvious endothermic peak at 916 °C and DTG maximum value at around 914 °C, is associated with decomposition of the sulfate

group in the precursor. Therefore, to obtain pure LaCuOS phase, 800 °C is recommended in this study. This thermal analysis result is consistent with that reported by Lian et al.[25]

3.4 Structural transformation of three precursors during calcining

Figure 4 shows the XRD patterns of three precursors and their corresponding calcination products at different temperatures. For the $La(NO_3)_3$-$NH_3{\cdot}H_2O$ system, it can be seen from left figure in **Figure 4** that the structure of the precursor changed during the calcination. The XRD analysis shows that the precursor and its calcination product at 200 °C are crystalline in structure with essential diffraction peaks. Unfortunately, there is no relevant crystal structure information in standard JCPD card database and their crystal structure is yet to be identified. After the precursor calcined at 400 °C, XRD pattern shows that the obtained diffraction pattern is consistent with the $LaONO_3$ data reported in JCPD cards No. 00-031-0665 and 00-028-0513. When the precursor was calcined at 600 °C, XRD analysis shows that the calcined product is composed of the $La_5O_7NO_3$ major phase (JCPDS card No. 00-038-0891) and a small amount of La_2O_3 phase (JCPDS card No.00-005-0602), indicating that the $LaONO_3$ phase has been completely converted to $La_5O_7NO_3$, and a small amount of $La_5O_7NO_3$ phase has begun to decompose into the La_2O_3 phase. Upon further increasing calcining temperature to 800 °C and 1000 °C, all the diffraction peaks of the calcination products can be indexed to the standard JCPDS card (No.00-005-0602) of the La_2O_3 phase. These results are also consistent with those obtained using the DTA-TG-DTG analysis. For the $CuSO_4$-$NH_3{\cdot}H_2O$ system, as shown in the middle figure in Figure 4, the precursor and its calcined product at 200 °C also have an unknown crystalline structure. However, after the precursor calcined at 400 °C, the XRD pattern shows that the diffraction peaks become a weak signal and gradually broaden, which corresponds to the destruction of the crystalline structure due to the removal of crystal water and hydroxyl groups. Similarly, when the precursor was calcined at 600 °C, the diffraction peaks of the CuO phase (JCPD card No. 00-010-1268) begin to appear in the XRD pattern and the diffraction peaks of $CuSO_4{\cdot}CuO$ still exist in the XRD pattern, which indicates that the $CuSO_4{\cdot}CuO$ does not completely transform to CuO at 600 °C. A further increase in the calcination temperature from 800 °C to 1000 °C leads to the generation of pure CuO phase. Finally, we discussed the phase-formation process of the synthesized precursor based on the $La(NO_3)_3$-$CuSO_4$-$NH_3{\cdot}H_2O$ system at different temperatures, as shown in the right figure in **Figure 4**. When the calcination temperature is less than or equal to 400 °C, the precursor has an amorphous structure without obvious diffraction peaks in the XRD pattern. When the precursor was calcined at 600 °C and 800 °C, the calcined product is composed of $La_2O_2SO_4$ (JCPD card No. 00-016-0501), $La_2(SO_4)_3$ (JCPD card No. 00-045-0904) and CuO (JCPD card No. 00-010-1268) phases according to the X-ray diffraction pattern. It is particularly important to note that the $La_2(SO_4)_3$ phase plays a crucial role in the formation of the LaCuOS target product. This will be discussed in the following section. With a further increasing of the calcination temperature to 1000 °C, the calcined product is only composed of $La_2O_2SO_4$ and

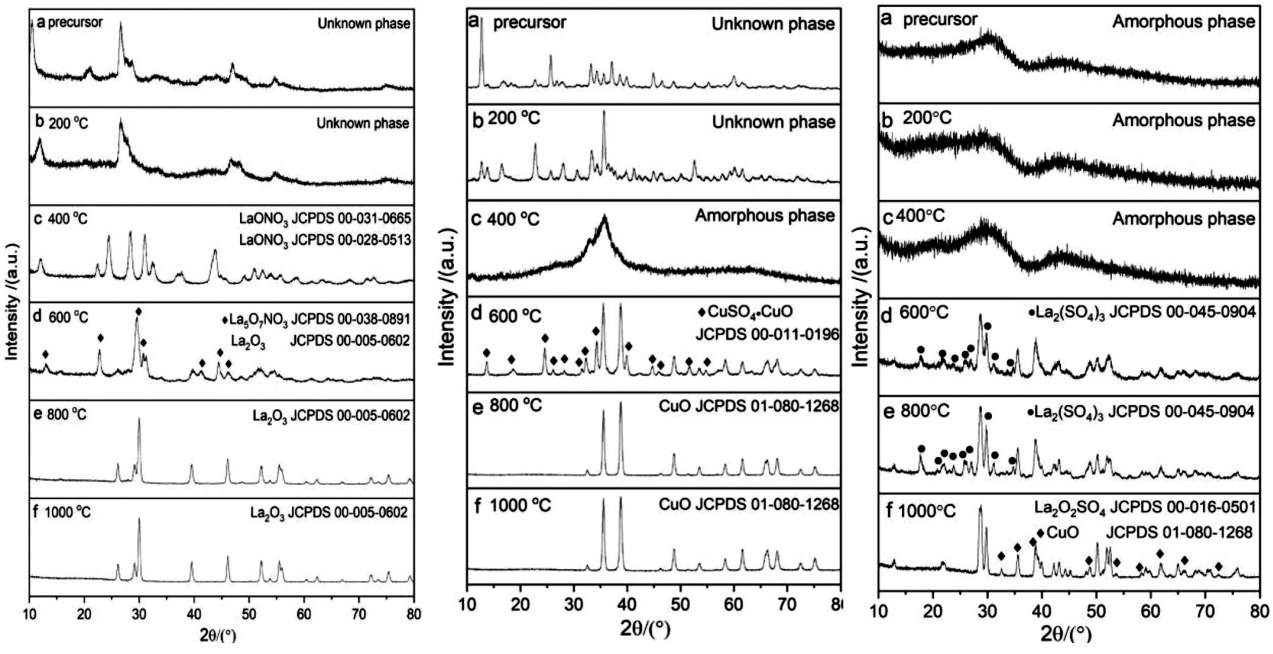

Figure 4: XRD patterns of three precursors and their corresponding calcination products at different temperatures. Left: $La(NO_3)_3$-$NH_3{\cdot}H_2O$ Middle: $CuSO_4$-$NH_3{\cdot}H_2O$ Right: $La(NO_3)_3$-$CuSO_4$-$NH_3{\cdot}H_2O$

CuO phases owing to the complete decomposition of $La_2(SO_4)_3$ to $La_2O_2SO_4$.

3.5 Transformation of the calcination product during reducing

To understand the formation mechanism of the LaCuOS phase and identify the appropriate reduction temperature for the 800 °C calcination product based on the $La(NO_3)_3$-$CuSO_4$-$NH_3{\cdot}H_2O$ system, DTA-TG-DTG was conducted from room temperature to 850 °C in argon and hydrogen atmosphere and the result is shown in **Figure 5**. The TG curve shows a continuous weight loss between room temperature and 850 °C with an overall weight loss of approximately 22.85 *w*/%. Little weight change can be observed at temperatures less than ≈420 °C on the TG curve, which indicates that the reduction reaction of the calcination product has not started before 420 °C. Within the temperature range of 420 °C to 500 °C, the TG curve has changed significantly and the weight loss is about 5.67 *w*/%. Meanwhile, a sharp peak at 436 °C on the DTG curve and an upward peak centered at 438 °C on the DTA curve appear, suggesting that the reduction reaction is an exothermic process. The above reactions are mainly related to the reduction of CuO and $La_2(SO_4)_3$ in the argon and hydrogen atmosphere, which corresponds to the following chemical equations (5) and (6).

$$2CuO + H_2 = Cu_2O + H_2O \quad (5)$$

$$La_2(SO_4)_3 + 2H_2 = La_2O_2SO_4 + 2SO_2 + 2H_2O \quad (6)$$

This result is also consistent with that obtained by XRD analysis in the following section. Moreover, when the reduction temperature is greater than 500 °C, a larger weight-loss process occurs according to the TG curve and the prominent peak at 688 °C and shoulder peak at 635 °C appear on DTG curve. A possible formation mechanism of LaCuOS is proposed according to relevant literature[28–29] and the following XRD analysis. The chemical reactions in the formation of LaCuOS can be expressed as follows:

$$2H_2 + SO_2 = 2H_2O + S \quad (7)$$

$$Cu_2O + H_2 = 2Cu + H_2O \quad (8)$$

$$La_2O_2SO_4 + 4H_2 = La_2O_2S + 4H_2O\uparrow \quad (9)$$

$$S + 2Cu + La_2O_2S = 2LaCuOS \quad (10)$$

To further verify the above thermal analysis result and investigate the phase evolution of the products at different temperature upon reduction, XRD analysis was conducted for two typical samples and the results are shown in **Figure 6**. When the 800 °C calcination product was reduced at 500 °C, the reduced product is composed of $La_2O_2SO_4$ (JCPD card No. 01-085-1534) and Cu_2O (JCPD card No. 01-077-0199) phases according to X-ray diffraction pattern (Figure 6a). The disappearance of $La_2(SO_4)_3$ in the reduced product indicates that it has been reduced to $La_2O_2SO_4$. Compared with Figure 6a, when the 1000 °C calcination product was reduced at 500 °C, the reduction product is also composed of $La_2O_2SO_4$ and Cu_2O. However, the XRD pattern shows the enhanced diffraction-peak intensity due to the high crystallinity of the 1000 °C calcination product. From

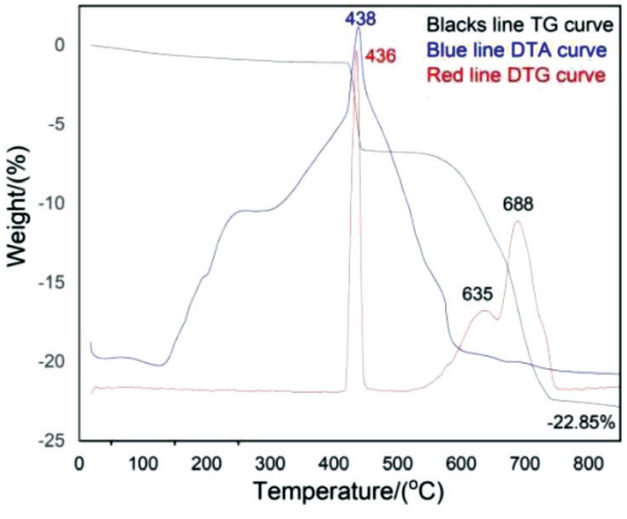

Figure 5: TG-DTG-DTA curves of the calcination product (800 °C, 2h) synthesized by the $La(NO_3)_3$-$CuSO_4$-$NH_3{\cdot}H_2O$ system

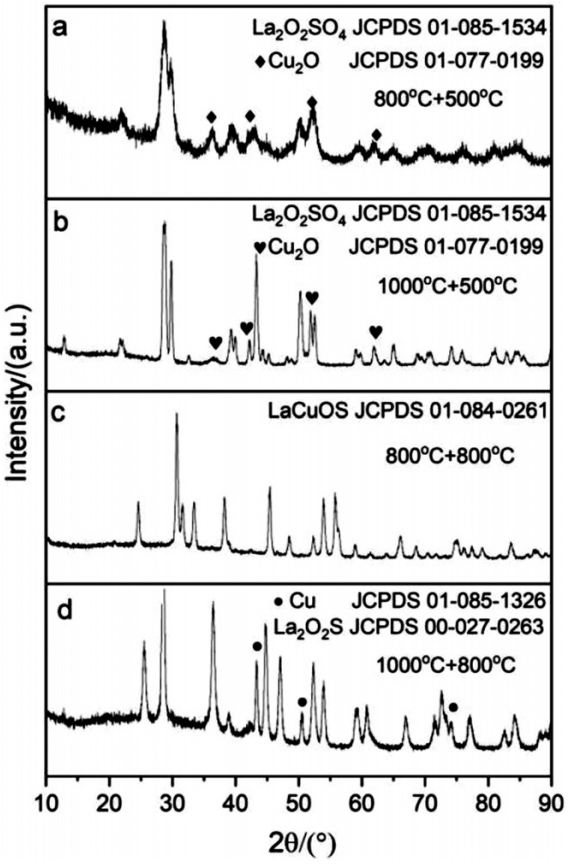

Figure 6: XRD patterns of the calcination products at different temperature under reducing atmosphere

Figure 6c, for the 800 °C calcination product, a further increasing reduction temperature of 800 °C results in the formation of pure LaCuOS phase owing to complete reaction of La_2O_2S, copper and sulfur according to the chemical equation (10). The phase evolution is consistent with the thermal analysis before (**Figure 5**). From **Figure 6d**, when the 1000 °C calcination product was reduced at 800 °C, all the diffraction peaks recorded from the reduction product can be indexed to hexagonal La_2O_2S (JCPD No. 01-027-0263) and copper (JCPD No. 01-085-1326) mixture. Thus, the selection of calcination products plays a decisive role in the formation of the target product, i.e., LaCuOS. The existence of $La_2(SO_4)_3$ in the calcined product is the key factor to obtain the final target product. Therefore, the calcination temperature of the synthesized precursor based on $La(NO_3)_3$-$CuSO_4$-$NH_3{\cdot}H_2O$ system should not exceed 800 °C in this study.

3.6 TEM morphologies and EDS analysis

Figure 7 shows TEM morphologies of a) the precursor, b) the calcination product (800 °C, 2h), c) the reduction product and d) EDS of the reduction product. It can be seen from **Figure 7a** that the precursor has a nearly spherical shape, a poor dispersion, a wide size distribution (20–50 nm). Moreover, it can be seen from **Figure 7b** that the calcination product inherits the morphology of the precursor, but it aggregates to some degree and becomes a bigger particle size (50–100 nm) due to the high-temperature calcination. Furthermore, shown in **Figure 7c**, for the reduction product, LaCuOS, the dispersivity becomes worse and the agglomeration phenomenon is more obvious compared with the calcination product (**Figure 7b**). Besides, the EDS analysis was conducted to gain the composition of the reduction product and the result is shown in **Figure 7d**, which demonstrates that the nano-sized agglomerates consist of lanthanum (La), copper (Cu), oxygen (O), and sulphur (S). The elemental ratios of La, Cu, O and S contained in the LaCuOS are quantified as 21.40:22.33:22.14:34.13. Although the ratio is not 1:1:1:1 due to the error of the EDS measurement method itself, it can be confirmed that the product is a quaternary compound containing La, Cu, O and S.

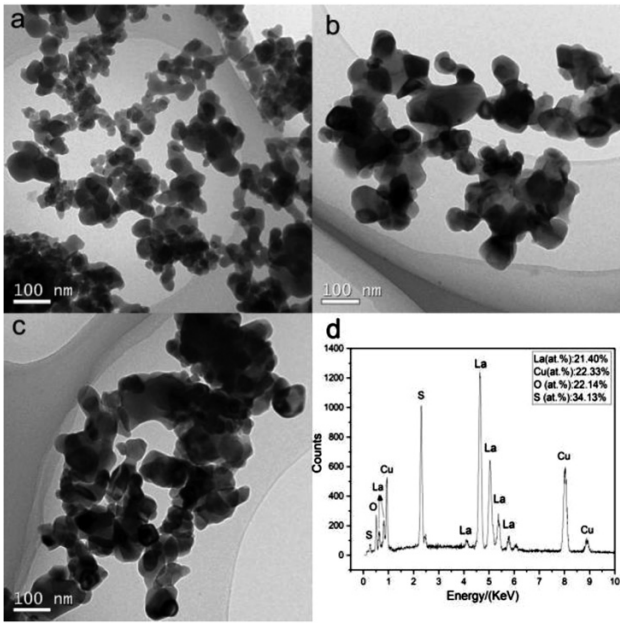

Figure 7: TEM morphologies of: a) the precursor, b) the calcination product (800 °C, 2h), c) the reduction product, d) EDS of the reduction product

4 CONCLUSIONS

In summary, LaCuOS nano-sized agglomerates were produced *via* a two-step synthesis of a co-precipitation and a reduction step, which use commercially available $La(NO_3)_3{\cdot}6H_2O$, $CuSO_4{\cdot}5H_2O$ and $NH_3{\cdot}H_2O$ as the starting materials. The present study shows that the appropriate pH value is 9.00 in the $La(NO_3)_3$-$CuSO_4$-$NH_3{\cdot}H_2O$ co-precipitation system. Moreover, the selection of calcination temperature plays a decisive role in the formation of LaCuOS and the calcination temperature of the synthesized precursor based on the $La(NO_3)_3$-$CuSO_4$-$NH_3{\cdot}H_2O$ system should not exceed 800 °C in order to obtain pure LaCuOS phase in this study. The as-prepared LaCuOS nano-aggregates have poor dispersion and a wide size distribution (50–100 nm). The two-step synthesis reported in this paper is an economical, convenient and *environmentally* friendly method to synthesize pure LaCuOS nano-sized agglomerates. In addition, the two-step synthesis method is also helpful for the preparation of other lanthanide copper oxychalcogenide.

Acknowledgements

This work was financially supported by the Provincial Education Department of Liaoning (No. lnqn202021).

5 REFERENCES

[1] D. O. Charkin, A. V. Urmanov, S. M. Kazakov, J. Alloys Compd, 516 (**2012**), 134

[2] S. Lardhi, A. Curutchet, L. Cavallo, M. Harb, T. L. Bahers, Phys. Chem. Chem. Phys., 19 (**2017**), 12321

[3] H. Matsushita, H. Takashima, A. Katsui, Phys. Stat. Sol., 8 (**2006**) 3, 2888

[4] J. Llanos, O. Pena, J. Solid State Chem., 178 (**2005**) 4, 957

[5] J. J. Ma, Q. Y. Liu, P. F. Liu, P. Zhang, B. Sanyal, T. Ouyang, B. T. Wang, Phys. Chem. Chem. Phys., 24 (**2022**), 21261

[6] H. Kamioka, H. Hiramatsu, H. Ohta, M. Hirano, App. Phys. Lett., 84 (**2004**) 6, 879

[7] K. Ueda, K. Takafuji, H. Hiramatsu, H. Ohta, T. Kamiya, M. Hirano, H. Hosono, Chem. Mater., 15 (**2003**) 19, 3692

[8] H. Kamioka, H. Hiramatsu, M. Hirano, K. Ueda, T. Kamiya, H. Hosono, Opt. Lett., 29 (**2004**) 14, 1659

[9] K. Ueda, K. Takafuji, H. Hosono, J. Solid State Chem., 170 (**2003**) 1, 182

[10] H. Sato, S. Nishimoto, K. Tsuji, K. Takase, H. Nakao, Y. Takahashi, T. Takano, K. Sekizawa, H. Negishi, S. Negishi, M. Nakatake, H. Namatame, M. Taniguchi, J. Alloys Compd, 408–412 (**2006**), 746
[11] D. O. Scanlon, J. Buckeridge, C. R. A. Catlow, G. W. Watson, J. Mater. Chem. C, 2 (**2014**) 17, 3429
[12] K. Takase, K. Sato, O. Shoji, Y. Takahashi, Y. Takano, K. Sekizawa, Y. Kuroiwa, M. Goto, App. Phys. Lett., 90 (**2007**) 16, 161916
[13] K. Ueda, S. Inoue, H. Hosono, N. Sarukura, M. Hirano, App. Phys. Lett., 78 (**2001**) 16, 2333
[14] A. Renaud, L. Cario, Y. Pellegrin, E. Blart, M. Boujtita, F. Odobel, S. Jobic, RSC Adv., 5 (**2015**) 74, 60148
[15] H. Yanagi , M. Kikuchi, K. Kim, H. Hiramatsu, T. Kamiya, M. Hirano, H. Hosono, Org. Electron. 9 (**2008**) 5, 890
[16] M. Palazzi, C. R. Acad. Sci. Paris, 292 (**1981**), 789
[17] Y. Goto, M. Tanaki, Y. Okusa, T. Shibuya, K. Yasuoka, M. Matoba, Y. Kamihara, App. Phys. Lett., 105 (**2014**) 2, 022104
[18] N. D. Zhang H. Gong, Cera. Int., 43 (**2017**) 8, 6295
[19] Y. Nakachi, K. Ueda, J. Cryst. Growth, 311 (**2008**) 1, 114
[20] Y. Takano, C. Ogawa, Y. Miyahara, H. Ozaki, K. Sekizawa, J. Alloys Compd, 249 (1997) 1–2, 221
[21] H. Hiramatsu, K. Ueda, H. Ohta, M. Orita, M. Hirano, H. Hosono, App. Phys. Lett., 81 (**2002**) 4, 598
[22] H. Hiramatsu, K. Ueda, H. Ohta, M. Hirano, T. Kamiya, H. Hosono, Thin Solid Films, 445 (**2003**) 2, 304
[23] H. Hiramatsu, K. Ueda, K. Takafuji, H. Ohta, M. Hirano, T. kamiya, H. hosono, Appl. Phys. A, 79 (**2004**), 1517
[24] N. D. Zhang, D. W. Shi, X. X. Liu, A. Annadi, B. S. Tang,T. J. Huang, H. Gong, Appl. Mater. Today, 13 (**2018**), 15
[25] J. B. Lian, N. N. Li, H. L. Wang, Y. Su, G. M. Zhang, F. Liu, Cera. Int., 42 (**2016**) 9, 11473
[26] L. H. Lee, Prog. Colloid Polym. Sci., 82 (**1990**), 337
[27] K. Huang, J. J. Wang, D. F. Wu, S. Lin, RSC Adv., 5 (**2015**) 11, 8455
[28] E. I. Sal'nikova, D. I. Kaliev, P. O. Andreev, Russ. J. Phys. Chem. A, 85 (**2011**) 12, 2121
[29] D. L. Murdock, G. A. Atwood, Ind. Eng. Chem., Process Des. Develop., 13 (**1974**) 3, 254